# Computational simulation of the multiphasic degeneration of the bone-cartilage unit during osteoarthritis via indentation and unconfined compression tests

**Seyed Shayan Sajjadinia**[1], **Mohammad Haghpanahi**[*1], and **Mohammad Razi**[2,3]

[1]School of Mechanical Engineering, Iran University of Science and Technology, Tehran 16846, Iran
[2]Department of Orthopedic Surgery, Iran University of Medical Sciences, Tehran 14665-354, Iran
[3]Department of Sports Medicine, Iran University of Medical Sciences, Tehran 14665-354, Iran

**Note**: This work is accepted for publication as a journal paper at

Sajjadinia, S. S., Haghpanahi, M. and Razi, M. (2019) "Computational simulation of the multiphasic degeneration of the bone-cartilage unit during osteoarthritis via indentation and unconfined compression tests," *Proceedings of the Institution of Mechanical Engineers, Part H: Journal of Engineering in Medicine*, 233(9), pp. 871–882.

www.doi.org/10.1177/0954411919854011



## Abstract

It has been experimentally proposed that the discrete regions of articular cartilage (AC), along with different subchondral bone (SB) tissues, known as the bone-cartilage unit (BCU), are biomechanically altered during osteoarthritis (OA) degeneration. However, a computational framework capturing all of the dominant changes in the multiphasic parameters has not yet been developed. This paper proposes a new BCU finite element (FE) model by combining several validated, nonlinear, depth-dependent, fibril-reinforced, and swelling models, which can computationally simulate the variations in the dominant parameters during OA degeneration by indentation and unconfined compression (UC) tests. The mentioned dominant parameters include the proteoglycan depletion, collagen fibrillar softening, permeability and fluid fraction increase for approximately non-advanced OA. The results depict the importance of SB tissues in fluid distribution within BCU by decreasing the fluid permeation and pressure (up to a maximum of 100 KPa) during OA, supporting the notion that SBs might play a role in the pathogenesis of OA. Furthermore, the OA composition-based studies shed light on the significant biomechanical role of the calcified cartilage (CC), which experienced a maximum change of 70 KPa in stress, together with relative load contributions of AC constituents during OA, in which the osmotic pressure bore around 70% of the loads after degeneration. To conclude, the new insights provided by the results reveal the significance of the multiphasic OA simulation and demonstrate the functionality of the proposed BCU model.

***Keywords*** Biomechanics · UMAT · multiphasic degeneration · finite element method · osteoarthritis · bone-cartilage unit · computational simulation

[*]Corresponding author at mhaghpanahi@iust.ac.ir

# 1 Introduction

Osteoarthritis (OA) is the most common form of the degenerative joint disease with sociological and financial impacts on health care systems [1, 2]. Although previous studies have characterized this condition as the articular cartilage (AC) wear and tear, contemporary studies suggest that OA is a whole knee joint disorder leading to pain and loss of function without chronic autoimmune mechanisms [3–5]. In particular, it was experimentally and also computationally observed that different subchondral bone (SB) tissues have a contributory role in the biomechanical and biochemical degenerative behavior of AC [6–9]. However, a small proportion of OA researches elaborated this key role [5, 10].

In the case of non-advanced OA, the bone-cartilage unit (BCU) permeability increases, and the AC constituents sustain damage depth-dependently [7,11,12]. The term BCU, as was firstly introduced by Lories and Luyten [5] and based on which some FE models were proposed [12, 13], consists of several hydrated soft and hard tissues, namely the AC, calcified cartilage (CC), subchondral cortical bone (SCB), and subchondral trabecular bone (STB).

Moreover, the AC itself has a multiphasic fibril-reinforced and heterogeneous structure, in which the proteoglycans and predominant type II collagen fibers govern the nonlinear and anisotropic compression-tension response of the tissue [14], which should not be underestimated [15]. The interplay of AC constituents gives rise to the osmotic pressure coming from biochemical factors [16–18] and excellent biotribological properties [19]. Also, the interstitial fluid pressurization induces a dominant-transient drag force, especially in AC, which potentially supports most of the applied load [19, 20]. Depending on the simulation procedures, incorporating all of the above-mentioned properties into a computational OA analysis is of high importance, yet it is challenging [21].

For the simulation of the multi-tissue pathogenesis of OA, which ideally involves whole knee joints, several FE simulations were carried out, although with a great deal of simplifying the constitutive equations [22, 23]. Nonetheless, they did not take into account the important osmotic pressure. Indeed, it is quite cumbersome to simulate the knee joint with its geometrical features and encompass an initially pre-stress state [24, 25]. However, by drastically simplifying geometries, the foregoing could be introduced, such as the tissue plugs in tissue-scale studies [13, 26].

In this study, a new BCU model was developed on the basis of the former well-established FE models. This computational model provides a more comprehensive description of BCU, enabling it to perform a multiphasic simulation of OA degeneration by comparing the healthy and degenerated BCU through a set of UC and indentation FE tests. The functionality of the proposed model has been assessed, which also elucidates the role of the constituents in OA. To our knowledge, no previous study has aimed at simulating such OA degeneration which takes account of all the dominant multiphasic factors. To this aim, the importance of such multiphasic simulation was assessed by comparing the results with their counterparts in the previous studies.

# 2 Materials and methods

## 2.1 Constitutive model

Basically, the AC could be modeled by standard biphasic theory described by Mow et al. [27]. However, the AC Cauchy stress is contributed by the non-fibrillar $\boldsymbol{\sigma}^{MAT}$, fibrillar $\boldsymbol{\sigma}^{COL}$, and glycosaminoglycan (GAG) $\boldsymbol{\sigma}^{GAG}$ parts. By considering the fluid pressure $p$, the AC total stress $\boldsymbol{\sigma}^{TOT}$ becomes

$$\boldsymbol{\sigma}^{TOT} = \boldsymbol{\sigma}^{COL} + \boldsymbol{\sigma}^{MAT} - \boldsymbol{\sigma}^{GAG} - p\mathbf{I} \tag{1}$$

The Cauchy stress of the tensile fibrillar and modified neo-Hookean non-fibrillar tensors was adapted from the previous research [28] as follows

$$\boldsymbol{\sigma}^{COL} = \frac{\phi_0^S}{J} \sum_{I=1}^{9} \left( \lambda^I \rho_C^I \left( E_0 + E_\varepsilon \varepsilon_F^I \right) \varepsilon_F^I \mathbf{n}^I \otimes \mathbf{n}^I \right) \qquad \varepsilon_F^I > 0 \tag{2}$$

$$\boldsymbol{\sigma}^{MAT} = \phi_0^S \left(1 - \rho_C^{TOT}\right) \left[ -\frac{lnJ}{6J} G_m \left( \frac{J\phi_0^S 3lnJ}{\left(\phi_0^S - J\right)^2} - 1 - 3\frac{J + \phi_0^S}{J - \phi_0^S} \right) \mathbf{I} + \frac{G_m}{J} \left( \mathbf{F}.\mathbf{F}^T - J^{2/3}\mathbf{I} \right) \right] \tag{3}$$

Where $\phi_0^S$ is the initial solid volume fraction parameter, $\mathbf{F}$ the deformation gradient tensor, $J$ the volumetric deformation, $G_m$ the shear modulus, $E_0$ and $E_\varepsilon$ the initial and strain-dependent collagen coefficients (due to collagen stiffening). Also, $\mathbf{n}^I$, $\lambda^I$, $\rho_C^I$, $\varepsilon_F^I$ are the current fibril direction, elongation, relative collagen fibril volume fraction, and logarithmic strain of the *Ith* fibril, respectively. This formulation ignores any AC viscosity as in our compression simulations, the only dominant transient response might be corresponding to the fluid pressurization [29].

The collagen network was assumed to be a combination of two large primary fibrils according to the arcade-like orientation [30, 31] and seven smaller secondary fibrils. Bundles of the dominant primary fibrils extend perpendicular from the subchondral surface, bend in opposite directions in AC middle zone (MZ) to become parallel to the AC surface. The secondary fibrils are orientated in the direction of each axis and between them. The fibril densities were derived by [32]

$$\rho_C^I = \begin{cases} \frac{\rho_C^{TOT}}{2C^F+7} C^F & \text{(Primary fibrils)} \\ \\ \frac{\rho_C^{TOT}}{2C^F+7} & \text{(Secondary fibrils)} \end{cases} \tag{4}$$

Where $C^F$ is a positive constant, and $\rho_C^{TOT}$ the depth-dependent total collagen volume fraction per total solid volume.

Furthermore, an extended two compartmental swelling stress model [33] was used to model the AC GAG constituent, as it potentially would provide a more accurate description of the degenerated AC than the ideal Donnan model [25, 34]. The GAG Cauchy stress is given by

$$\boldsymbol{\sigma}^{GAG} = \hat{\alpha}_1 \left(\frac{1}{J}\right)^{\alpha_2} \mathbf{I} \tag{5}$$

Where $\hat{\alpha}_1$ and $\alpha_2$ are GAG material constants.

As the AC finite strains may lead to the void ratio $e$ changes, a depth- and strain-dependent permeability function was chosen [35–38]

$$k = k_0 \left(\frac{e}{e_0}\right)^{\kappa} exp\left(\frac{M}{2}\left[\left(\frac{1+e}{1+e_0}\right)^2 - 1\right]\right) \tag{6}$$

Where $k_0$ is the zero-strain permeability, $e_0$ the initial void ratio, $\kappa$ and $M$ the material constants.

On the other hand, the subchondral regions were approximated by a biphasic mixture with an isotropic elastic solid phase and equivalent fluid phase [12]. Therefore, they are governed by their Young's modulus $E_b$ and Poisson's ratio $\nu_b$ and permeability $k_b$ parameters. A comprehensive list of material properties is shown in Table 1.

### 2.2 Implementation

The BCU FE model was solved with the aid of the soil consolidation theory in Abaqus (v6.14, Simulia). However, the AC effective solid parts should be implemented via a user-defined material (UMAT) subroutine. Before running the analysis (step 0), the continuous depth-dependent material parameters had been calculated in each AC integration point from the normalized depth parameter ($z$) by the SDVINI subroutine. Subsequently, the calculated parameters were transferred to the UMAT subroutine by the state variables (STATEV). Then, a static (equilibrium) step was run to account for the pre-stress effects on the AC solid matrix due to GAG molecules reactions (Figure 1).

As the UMAT subroutine makes use of Newton's method for the sake of FE linearization, the fourth-order consistent Jacobian tensor should be defined, which is a function of the right Cauchy-Green deformation tensor $\mathbf{C}$. This tensor is defined as

$$\mathbf{C} = \mathbf{F}^T \cdot \mathbf{F} \tag{7}$$

To derive the consistent Jacobian tensor ${}^4c_{ijkr}$, the following equation was suggested [54] in indicial notation

Table 1: BCU material parameters: The BCU permeability and SB parameters were collected by Stender et al. [12] from previous works [7, 39–46]. Taffetani et al. [47] measured GAG material coefficients depth-dependently via the procedure proposed by Stender et al. [25]. Also, the fibrillar and non-fibrillar material coefficients of the healthy AC was gathered by Wilson et al. [28] from former studies [32, 48–50]. The changes in softened AC were adapted from previous works [51–53]. Generally, these properties were supposed to simulate a generalized BCU model rather than a specific type.

| Material Parameter | Intact | Degenerated ($\mu$m) |
|---|---|---|
| $E_\varepsilon$ (MPa) | 3670 | 917.5 |
| $E_0$ (MPa) | 4.63 | |
| $G_m$ (MPa) | 0.723 | |
| $C^F$ (-) | 3.009 | |
| $\alpha_2$ (-) | 3.22 | |
| $\hat{\alpha}_1$ (MPa) | Layer 1: 0.005 | |
| | Layer 2: 0.010 | |
| | Layer 3: 0.025 | |
| | Layer 4: 0.035 | |
| | Layer 5: 0.042 | |
| | Layer 6: 0.048 | |
| | Layer 7: 0.053 | |
| | Layer 8: 0.058 | |
| | Layer 9: 0.060 | |
| $\rho_c^{tot}$ (-) | $1.4z^2 + 1.1z + 0.59$ | |
| $\phi_0^S$ (-) | $0.1 + 0.1z$ | $0.05 + 0.1z$ |
| $k_0$ (mm$^2$.s$^{-1}$/MPA) | SZ: $6.81 \times 10^{-3}$ | SZ: $4.55 \times 10^{-3}$ |
| | MZ: $2.16 \times 10^{-3}$ | MZ: $1.46 \times 10^{-3}$ |
| | DZ: $0.74 \times 10^{-3}$ | DZ: $0.5 \times 10^{-3}$ |
| $M$ (-) | SZ: 5.48, MZ: 5.49, DZ: 7.38 | |
| $k_b$ (mm$^2$.s$^{-1}$/MPA) | 140 | 90 |
| $E_b$ (MPa) | CC: 320, SCB: 3900, STB: 1019 | |
| $\nu_b$ (-) | 0.03 | |

$$ {}^4c_{ijkr} = \frac{1}{2}\left(\delta_{ri}\sigma_{kj}^{EFF} + \delta_{kj}\sigma_{ir}^{EFF} + \delta_{ki}\sigma_{rj}^{EFF} + \delta_{rj}\sigma_{ik}^{EFF}\right) + {}^4\widetilde{c}_{ijkr} \tag{8} $$

Where $\delta$ is the Kronecker delta, and ${}^4\widetilde{c}_{ijkr}$ the fourth-order spatial elasticity tensor, which is

$$ {}^4\widetilde{c}_{ijkr} = \frac{1}{J}\left[F_{ip}F_{jq}F_{kl}F_{rs}\left({}^4\widetilde{C}_{pqls}\right)\right] \tag{9} $$

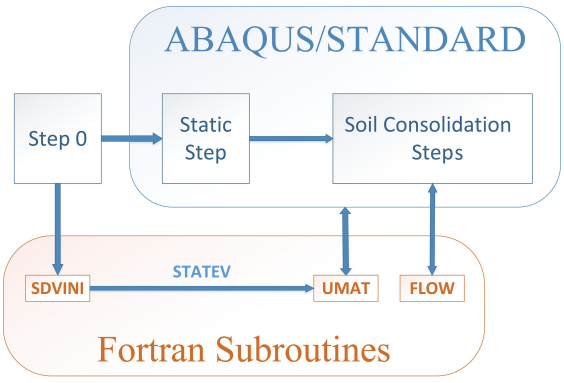


Figure 1: The interplay between Abaqus steps and different Fortran subroutines.

Also, ${}^4\widetilde{C}_{pqls}$ is the corresponding fourth-order material elasticity tensor, which should be computed for each of the AC solid parts by

$$ {}^4\widetilde{\mathbf{C}} = 2\frac{\partial \mathbf{S}}{\partial \mathbf{C}} \tag{10} $$

Where $\mathbf{S}$ is the 2nd Piola–Kirchhoff stress tensor, which is related to the Cauchy stress tensor by

$$ \mathbf{S} = J\mathbf{F}^{-1} \cdot \sigma \cdot \mathbf{F}^{-T} \tag{11} $$

Therefore, the fourth-order elasticity tensor should be derived for each part by the above-mentioned equations as follows

$$ {}^4\widetilde{c}_{ijkr} = \frac{1}{2}\left(\delta_{ri}\sigma^{EFF}_{kj} + \delta_{kj}\sigma^{EFF}_{ir} + \delta_{ki}\sigma^{EFF}_{rj} + \delta_{rj}\sigma^{EFF}_{ik}\right) + {}^4\widetilde{c}^{COL}_{ijkr} + {}^4\widetilde{c}^{MAT}_{ijkr} + {}^4\widetilde{c}^{GAGs}_{ijkr} \tag{12} $$

Where ${}^4\widetilde{c}^{COL}_{ijkr}$, ${}^4\widetilde{c}^{MAT}_{ijkr}$, ${}^4\widetilde{c}^{GAGs}_{ijkr}$ are respectively the fibrillar, non-fibrillar, and GAG spatial elasticity tensors. The latter was previously derived as [47]

$$ {}^4\widetilde{c}^{GAG}_{ijkr} = \hat{\alpha}_1 \left(\frac{1}{J}\right)^{\alpha_2} \left[(\alpha_2 - 1)\,\delta_{ij}\delta_{kr} + \delta_{ik}\delta_{jr} + \delta_{ir}\delta_{jk}\right] \tag{13} $$

The other constituent elasticity tensors were derived in Appendix as

$$ {}^4\widetilde{c}^{COL}_{ijkr} = \frac{\phi^S_0}{J}\sum_{I=1}^{9}\left(\rho^I_C\lambda^I\left[E_0 + 2E_\varepsilon\varepsilon^I_F - \left(E_0 + E_\varepsilon\varepsilon^I_F\right)\varepsilon^I_F\right] n^I_i n^I_j n^I_k n^I_r\right) \tag{14} $$

$$ \begin{aligned} {}^4\widetilde{c}^{MAT}_{ijkr} = \phi^S_0\left(1-\rho^{TOT}_C\right)\Bigg(&\frac{G_m}{J}\left(J^{2/3} + \frac{lnJ}{6}\left[\frac{3n_{s,0}}{J-n_{s,0}}\left(\frac{JlnJ}{J-n_{s,0}} - 2\right) - 4\right]\right)\left(\delta_{ik}\delta_{jr} + \delta_{ir}\delta_{jk}\right) \\ &- \frac{G_m}{2}\left(\frac{4J^{2/3} - 4 + \frac{3\phi^S_0}{J-\phi^S_0}\left(\frac{JlnJ}{J-\phi^S_0} - 2\right)}{3J} + \frac{(lnJ-1)\,\phi^S_0 lnJ}{\left(J-\phi^S_0\right)^2}\right)\delta_{ij}\delta_{kr}\Bigg) \end{aligned} \tag{15} $$

### 2.3 Simulations

To investigate the OA multiphasic degeneration effects, the tests were simulated for the healthy and degenerated BCU models by an approach similar to the previous studies [12,53], where the thicknesses of the AC superficial zone (SZ), MZ and deep zone (DZ), as well as CC, SCB, and STB regions were assumed to be 1.5mm, 5.0mm, 3.5mm, 0.05mm, 10mm, 10mm, respectively. Also, all the dominant parameters were altered during the non-advanced OA according to the recent study [11].

The UC test was simulated by 620 four-node axisymmetric quadrilateral, bilinear displacement and pore pressure elements with full integration (CAX4P). The nodal displacements at the bottom rigid impermeable platen were confined. The BCU, 10mm in diameter, was axially compressed by a rigid impermeable platen up to 1% strain. After relaxation, an additional 5% strain at a ramp-strain rate of $0.001\text{s}^{-1}$ took place, and then the platen was held unchanged to allow for full relaxation; meanwhile, the reaction force was recorded.

As to the indentation test, 1722 identical elements were utilized. The nodes at the bottom of BCUs were completely constrained. The BCU diameter was increased to 70mm to prevent any edge effects in AC. The indentation loading was applied by a 5% strain of the impermeable indenter (Figure 2) at a strain rate of $0.05\text{s}^{-1}$, with subsequent unloading back to the initial location during 2s, while the reaction force was recorded. The impermeable indenter, 25mm in diameter, was modeled with a small fillet of radius 0.3mm at the sharp corner in order to avoid the induced stress concentration. The nodal displacements at the bottom impermeable plane of the BCUs were confined, while a biphasic contact condition was prescribed, in which the free fluid flow was allowed in the top BCU surface that is not in contact. This contact condition was prescribed by a FLOW subroutine, which requires identifying the seepage coefficient and reference sink

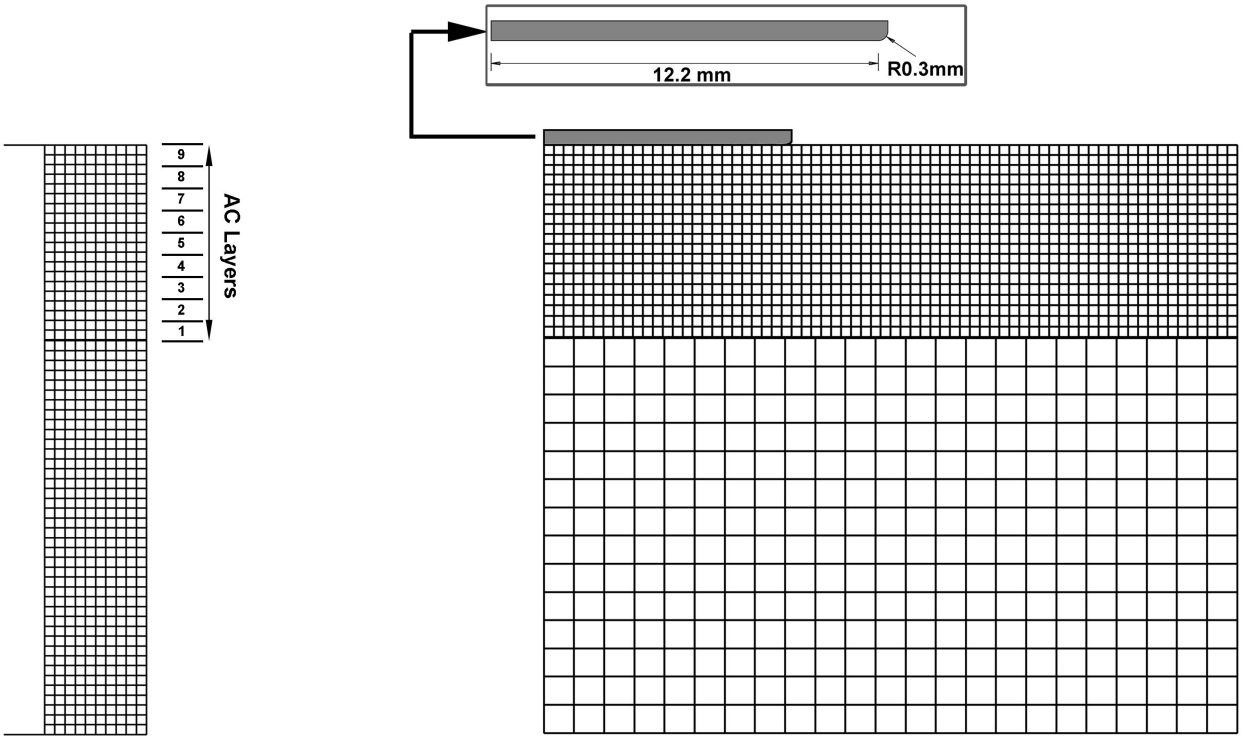


Figure 2: Axisymmetric FE models for UC simulation (left) and indentation simulation (right).

pressure parameters. For our material constitutive equations, the foregoing parameters were assumed to be 1mms$^3$/N.s and 0, respectively [55].

As explained in the preceding section, a static step was implemented for 1s before implementing the main simulations (Figure 1). Following this step in the indentation tests and the first relaxation in the UC tests, the vertical Cauchy stresses in the BUC parts were calculated to evaluate the functionality of the proposed model. Also, the displacements of the nodes at the symmetry axis of all of the models were confined in the radial direction while zero pore pressure was imposed on the radial boundaries.

In addition to implementing a mesh refinement study and comparing the results of this study with the previous experimental data, two other experimental tests were simulated once again by the proposed model to evaluate the validity of the model. Accordingly, a UC test [56], plus a confined compression experiment [57], which was also replicated by another validated FE model [28], were implemented. Readers are referred to the corresponding papers for a more detailed description of the tests.

## 3 Results

### 3.0.1 Simulations

Figure 3 represents the results of the pore pressure and fluid velocity vector for the healthy and degenerated BCU in the indentation test. While a 30% decrease in the fluid velocity is discernible in subchondral regions, the pore pressure decreased by a maximum of around 100KPa in AC. This test shows a huge diminished peak reaction force during OA degeneration (Figure 4). Also, the mesh refinement study of the reaction force demonstrates sufficient mesh convergence by roughly a 50% reduction of the element numbers. Another point to consider is that the AC boundary near CC involves some distortions due to the AC pre-stress condition, which produced oscillating values. These inaccuracies are far from the region of interest and therefore did not interrupt the validity of the results.

The contributions of the AC phases, near the subchondral zones, to vertical load sharings were depicted in percent (Figure 5). During OA, the load support was mainly shifted from the fluid pressure to the other AC phases, particularly the osmotic pressure, which also decreased depth-wisely (Figure 6).

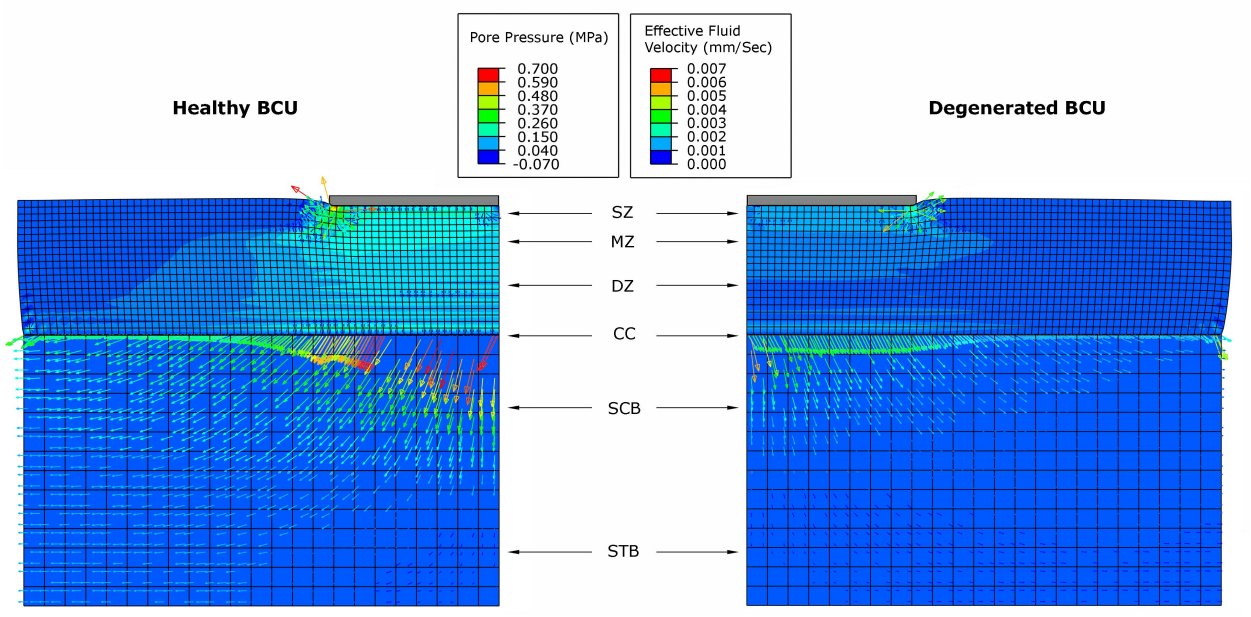


Figure 3: FE indentation simulation results for interstitial pore pressure and fluid velocity at peak load (just before the unloading step).

The recorded reaction forces in both compression tests declined by roughly 50% after OA while the stresses in the AC parts mainly decreased, with the exception of the fibrillar stresses, which increased after OA (10KPa in peak loads), and the non-fibrillar stresses, which were more or less zero in all tests (Figure 7). Also, the recorded stresses in subchondral regions fell after OA, where the CC and STB respectively correspond to the lowest and highest stresses in UC tests, and these regions respectively contributed the most and the least to the load bearings in the indentation tests (Figure 8). The magnitudes of the osmotic pressure and non-fibrillar stress did not substantially vary during each different analysis; meanwhile, the fluid and fibrillar phases experienced upward and downward trends, respectively. After OA, the fluid part witnessed the most significant falls in stress (around 30KPa in UC and 80KPa in indentation tests), and the fibrillar part went up by around 10KPa in both tests at peak loads. During unloading, the values of fluid pressure, unlike other BCU parts, did not follow the same paths as the loading steps to reach zero and experienced the maximum

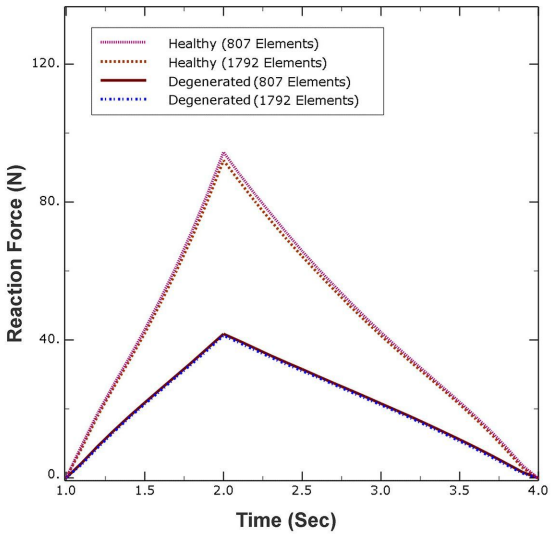


Figure 4: Plots of reaction force vs. time for the indentation test.

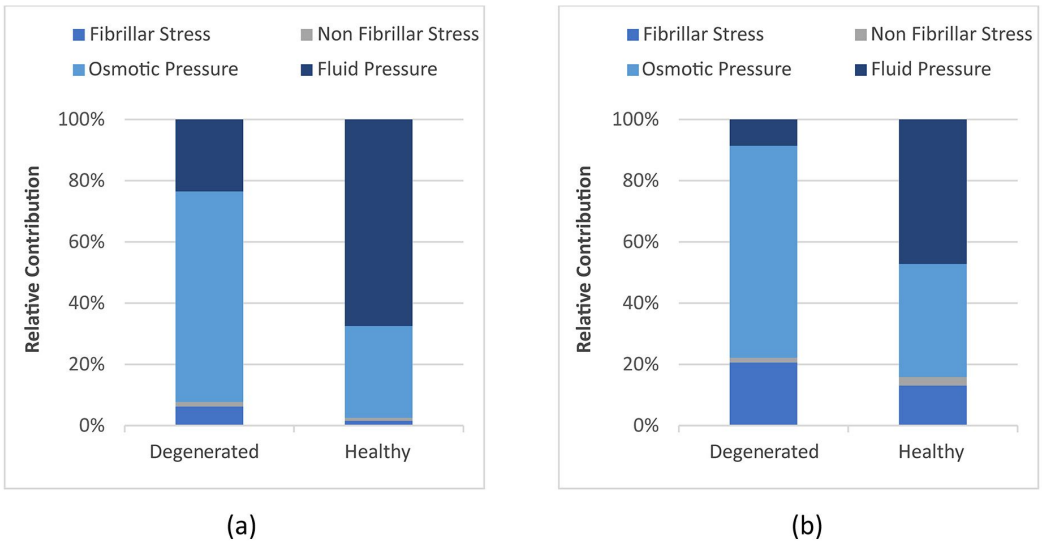


Figure 5: Contribution of AC components to normal load sharing in the DZ near the SBs at peak loads in (a) UC and (b) indentation tests.

decreases of roughly 40KPa and 10KPa before and after OA, respectively. During stress relaxation, the stresses in the fluid and CC parts first peaked then reduced, whereas the stresses in the other AC phases did not vary dramatically, and the subchondral stresses went down. Among peak stresses in different subchondral regions, the CC saw the most drastic drops in stress during OA (70 and 53KPa in indentation and UC tests, respectively).

### 3.0.2 Validation tests

During the UC test, the model could predict the response in the range of the maximum strain of this study (around 10%). Further deformation of the tissue, led to an approximately maximum error of 15% (Figure 9).

The confined compression results represent similar trends in the stress-strain behavior of the tissue constituents, while a roughly fixed difference in the osmotic pressure is observable (around 20KPa), originated from the

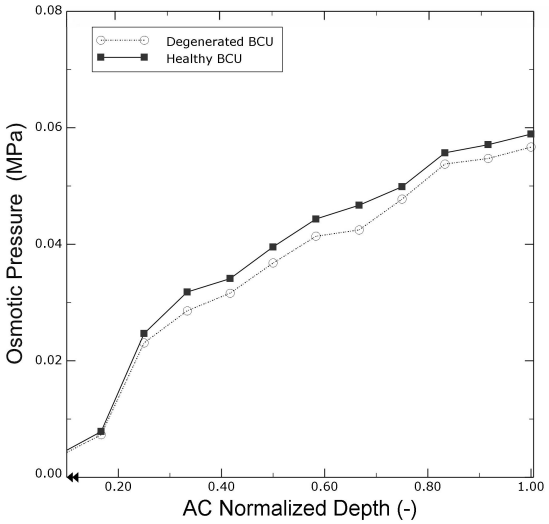


Figure 6: Plots of osmotic pressure vs. AC normalized depth (z) for indentation analysis at peak load.

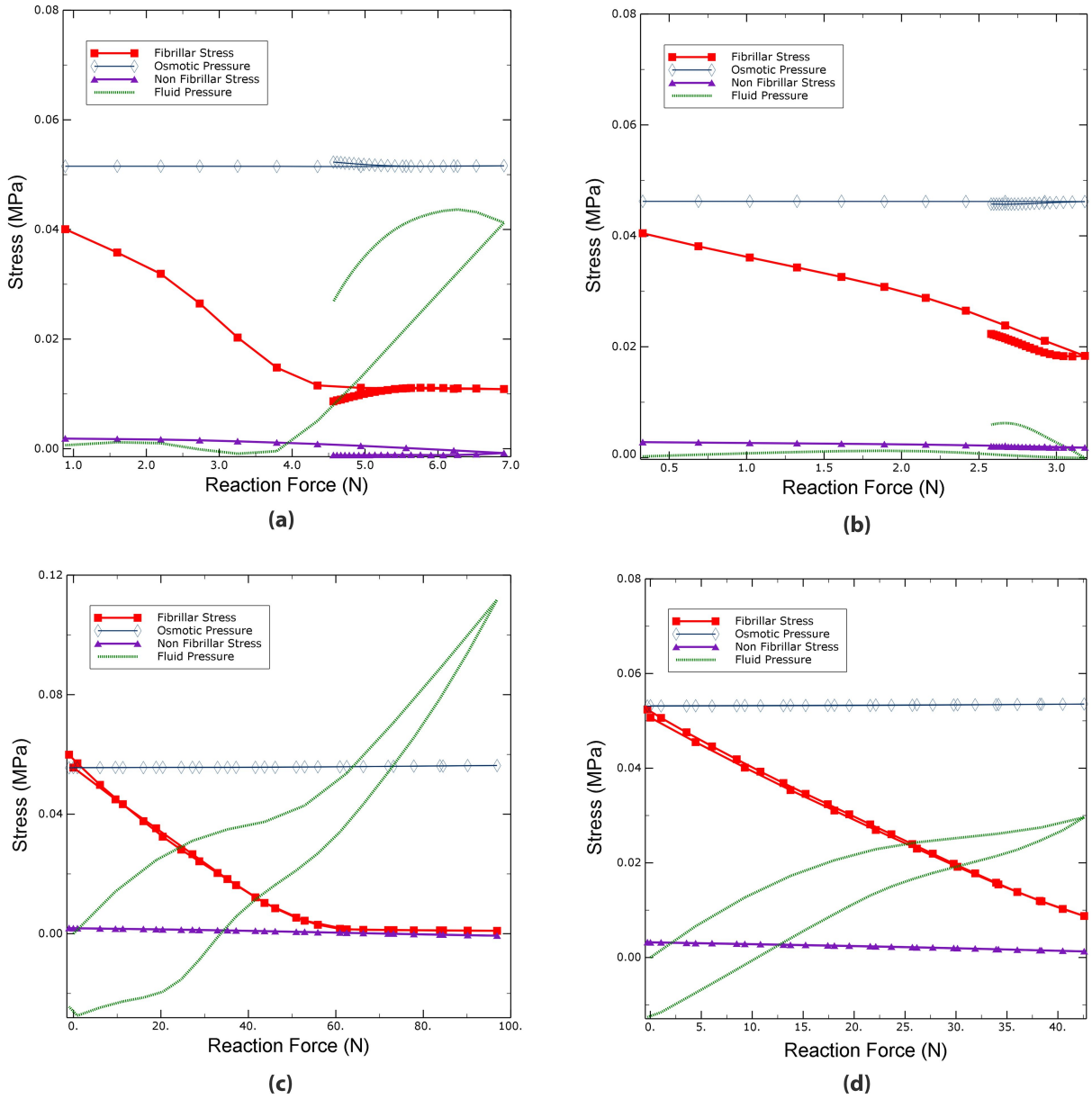


Figure 7: Stress in different phases of AC, near the SBs, as a function of recorded reaction force during UC tests on (a) healthy and (b) degenerated BCUs, plus indention tests on (c) healthy and (d) degenerated BCUs.

difference in the GAG formulations. The total stress results, however, are similar to the previous numerical and experimental data (Figure 10).

## 4 Discussion

This study proposed a BCU FE model by incorporating some of the validated models [12, 28, 33] to conduct a multiphasic simulation of the non-advanced OA during a set of UC and indentation tests. The degeneration was studied by altering the dominant changing parameters, which are comprised of the collagen softening, permeability and fluid fraction increase. The principal alterations during OA degeneration typically include simultaneous proteoglycan and collagen depletion [11]. Proteoglycans depletion increases the BCU permeability

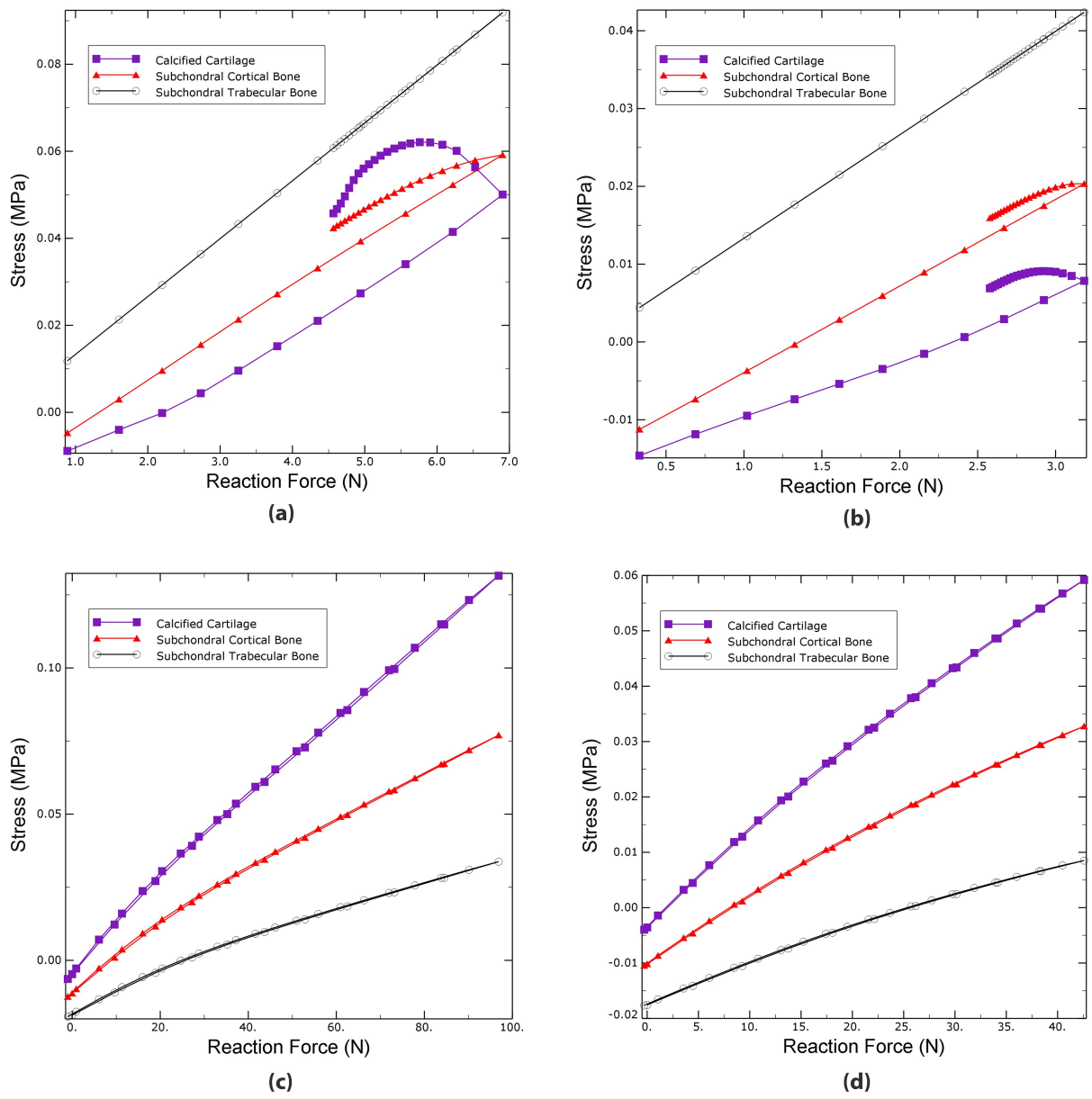


Figure 8: Stress in subchondral regions as a function of recorded reaction force during UC tests on (a) healthy and (b) degenerated BCUs, plus indention tests on (c) healthy and (d) degenerated BCUs.
Note: The simulation method was aimed at assessing the functionality of BCU multiphasic model, and the result would be different in advanced OA or different loading conditions.

and AC fluid fraction, and it alters the osmotic pressure and solid matrix stiffness [52]. The latter case could be neglected, considering that the non-fibrillar constituent bears inappreciable importance in our simulations [18] (Figure 5). The proteoglycan depletion is discernible only in the SZ during early OA [11]. However, this zone involves lesser osmotic pressure [18] (Figure 6). Therefore, the osmotic material parameters assumed constant during the simulations.

In both of the tests, the OA degeneration reduced the AC osmotic pressure, while its load sharing contributions were dramatically increased, despite the overall osmotic pressure reduction (Figure 7). The fibrillar stress contributions increased, which is interesting as this part was softened, implying that the degeneration transferred more loads from the fluid phase to the fibrillar phase. As the tests were carried out by the

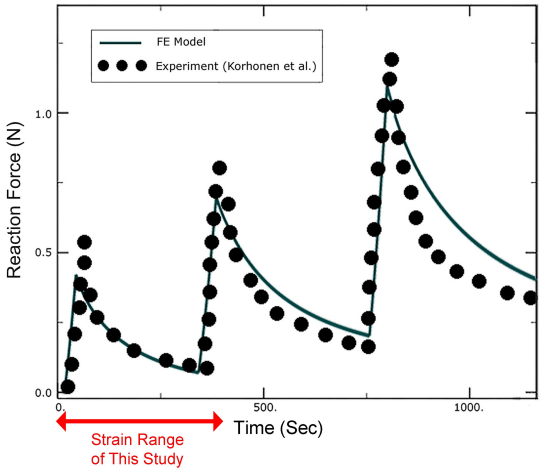


Figure 9: Plot of reaction force vs. time in validation UC experiment conducted by Korhonen et al. [56].

displacement control less than 10% strain, the BCU stresses witnessed an unsurprising reduction in stress. Also, CC involves the highest stress variations, implying that CC might be the most important part of subchondral tissues, which is in agreement with the previous experimental observations [7, 11] (Figure 8).

In the Indentation simulation, the reaction force decreased after OA (Figure 4), which is in contrast to the previous FE simulation [12], as they only considered the permeability increase. Therefore, the recording reaction force was governed by the solid matrix softening in lieu of the 'short circuit' effect, which could surprisingly increase the elasticity in some particular situations [12]. The similar reduction in the reaction forces was also reported in the previous experimental AC study [58]. Additionally, in agreement with some experimental observations [7, 59], this simulation put the emphasis on the importance of the mass transport in SBs, considering that the degeneration can severely reduce the fluid permeation through SBs (Figure 3). The result would have been totally different if our model only had encompassed the permeability increase [12]. These conflicting results show the importance of a totally multiphasic simulation.

The accuracy of the proposed FE model was evaluated by comparison of the data from previous studies as well as implementing separate studies with this model. First and foremost, the previous validated FE study [18] determined the relative contributions of the healthy AC parts to load bearings under similar compression tests, in which the results for the AC DZ zones indicate that the fluid pressure contributed the

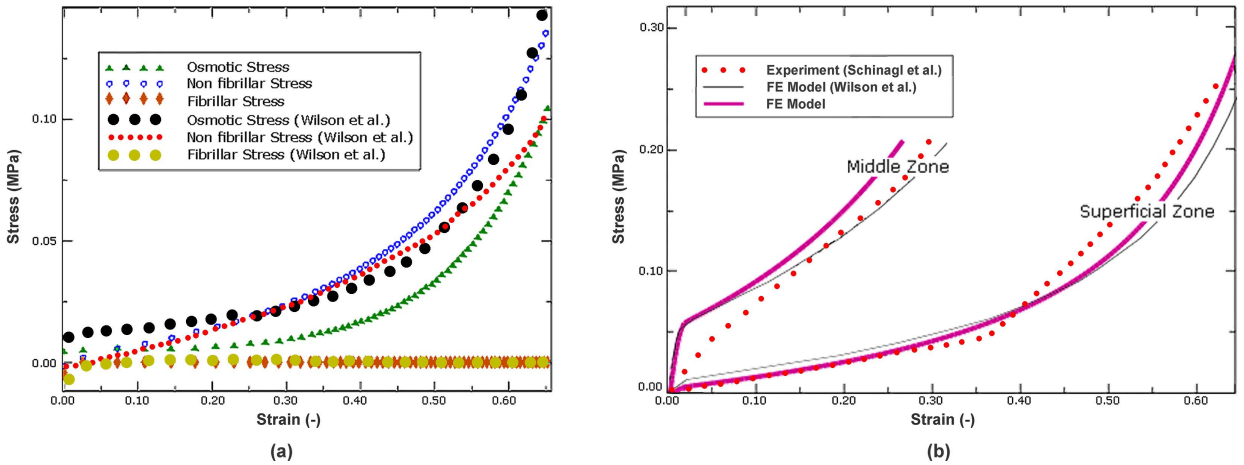


Figure 10: Plots of stress-strain behavior, measured from validation simulation of confined compression, proposed by Schinagl et al. [57] and replicated by Wilson et al. [28], in terms of (a) constituent stresses in the AC upper layers and (b) effective stresses.

most (73% in indentation and 63% in UC), and the remaining loads were mostly supported by the osmotic pressure. These findings are very analogous to the results of the present BCU model (Figure 5), although their fluid pressure parameters took more loads (around a maximum of 20%). Such a difference could be explained by the higher strain rates of the previous study, which can turn some of the osmotic pressure to fluid pressure [18]. Secondly, replication of two other experimental tests, including a UC [56] (Figure 9) and confined compression tests [57] (Figure 10), verified the general model fidelity. Finally, the mesh refinement studies were conducted in the indentation simulation, because of the mesh distortions near the boundary, which verified the computational accuracy (Figure 4).

Although this study improved on the general BCU model, it still has some limitations. Firstly, the loading conditions were deliberately chosen in compliance with the previous similar study [60] for the sake of comparison, which did not include all the physiological loads, such as the rotational or shear load types. Moreover, the SB model incorporated a general material description of SBs and the changes in permeability during OA, giving a better qualitative picture of the OA process in this region in comparison to previous models. Nonetheless, such a general model of SBs is another limitation of this study, as it did not encompass the location-dependent alterations in the geometry and biomaterial parameters of SBs [9], which can quantitatively affect the recorded parameters in subchondral parts [9]. The future studies should be directed toward the simulations with more load conditions along with further details of the material behavior of the tissue [61–65].

In conclusion, the proposed FE model provides some different results in comparison to its simpler counterparts, showing the importance of the multiphasic simulation of BCU OA. In particular, the simulation might reinforce the notion that different SBs play a role in the pathogenesis of OA by reducing the overall fluid permeation. Also, it is shown that the BCU dominant parameters highly influence the OA degeneration, and the relative contribution of the fibrillar part might surprisingly increase by collagen softening. These new results demonstrate the functionality of the proposed general BCU model.

## Acknowledgements

We would like to sincerely express our gratitude to Dr. Hajar Razi (Max Planck Institute of Colloids and Interfaces) for providing valuable information and recommendations regarding the biomedical aspects.

## Declaration of conflicting interests

The authors declare no conflict of interest.

## References

[1] A. Chen, C. Gupte, K. Akhtar, P. Smith, and J. Cobb, "The global economic cost of osteoarthritis: How the uk compares," *Arthritis*, vol. 2012, p. 1–6, Oct 2012.

[2] C. G. Helmick, D. T. Felson, R. C. Lawrence, S. Gabriel, R. Hirsch, C. K. Kwoh, M. H. Liang, H. M. Kremers, M. D. Mayes, P. A. Merkel, and et al., "Estimates of the prevalence of arthritis and other rheumatic conditions in the united states. part i," *Arthritis and Rheumatism*, vol. 58, no. 1, p. 15–25, 2008.

[3] K. D. Brandt, E. L. Radin, P. A. Dieppe, and L. Van De Putte, "Yet more evidence that osteoarthritis is not a cartilage disease," *Annals of the Rheumatic Diseases*, vol. 65, p. 1261–1264, Sep 2006.

[4] D. T. Felson and T. Neogi, "Osteoarthritis: Is it a disease of cartilage or of bone?," *Arthritis and Rheumatism*, vol. 50, p. 341–344, Feb 2004.

[5] R. J. Lories and F. P. Luyten, "The bone–cartilage unit in osteoarthritis," *Nature Reviews Rheumatology*, vol. 7, p. 43–49, Jan 2011.

[6] D. B. Burr, "Anatomy and physiology of the mineralized tissues: Role in the pathogenesis of osteoarthrosis," *Osteoarthritis and Cartilage*, vol. 12, p. 20–30, Jan 2004.

[7] J. Hwang, W. C. Bae, W. Shieu, C. W. Lewis, W. D. Bugbee, and R. L. Sah, "Increased hydraulic conductance of human articular cartilage and subchondral bone plate with progression of osteoarthritis.," *Arthritis and rheumatism*, vol. 58, p. 3831–42, Dec 2008.

[8] R. C. Paietta, E. L. Burger, and V. L. Ferguson, "Mineralization and collagen orientation throughout aging at the vertebral endplate in the human lumbar spine," *Journal of Structural Biology*, vol. 184, p. 310–320, Sep 2013.

[9] M. S. Venäläinen, M. E. Mononen, J. S. Jurvelin, J. Töyräs, T. Virén, and R. K. Korhonen, "Importance of material properties and porosity of bone on mechanical response of articular cartilage in human knee joint—a two-dimensional finite element study," *Journal of Biomechanical Engineering*, vol. 136, no. 12, p. 121005, 2014.

[10] H. Madry, C. N. van Dijk, and M. Mueller-Gerbl, "The basic science of the subchondral bone," *Knee Surgery, Sports Traumatology, Arthroscopy*, vol. 18, no. 4, p. 419–433, 2010.

[11] S. Saarakkala, P. Julkunen, P. Kiviranta, J. Mäkitalo, J. S. Jurvelin, and R. K. Korhonen, "Depth-wise progression of osteoarthritis in human articular cartilage: investigation of composition, structure and biomechanics," *Osteoarthritis and Cartilage*, vol. 18, no. 1, p. 73–81, 2010.

[12] M. E. Stender, R. A. Regueiro, and V. L. Ferguson, "A poroelastic finite element model of the bone–cartilage unit to determine the effects of changes in permeability with osteoarthritis," *Computer Methods in Biomechanics and Biomedical Engineering*, vol. 20, p. 319–331, Sep 2017.

[13] M. E. Stender, R. D. Carpenter, R. A. Regueiro, and V. L. Ferguson, "An evolutionary model of osteoarthritis including articular cartilage damage, and bone remodeling in a computational study," *Journal of Biomechanics*, vol. 49, no. 14, p. 3502–3508, 2016.

[14] J. S. Jurvelin, M. D. Buschmann, and E. B. Hunziker, "Mechanical anisotropy of the human knee articular cartilage in compression," *Proceedings of the Institution of Mechanical Engineers, Part H: Journal of Engineering in Medicine*, vol. 217, p. 215–219, Mar 2003.

[15] S. M. Hosseini, Y. Wu, K. Ito, and C. C. Van Donkelaar, "The importance of superficial collagen fibrils for the function of articular cartilage," *Biomechanics and Modeling in Mechanobiology*, vol. 13, no. 1, p. 41–51, 2014.

[16] J. Katta, T. Stapleton, E. Ingham, Z. M. Jin, and J. Fisher, "The effect of glycosaminoglycan depletion on the friction and deformation of articular cartilage," *Proceedings of the Institution of Mechanical Engineers, Part H: Journal of Engineering in Medicine*, vol. 222, p. 1–11, Jan 2008.

[17] R. K. Korhonen and J. S. Jurvelin, "Compressive and tensile properties of articular cartilage in axial loading are modulated differently by osmotic environment," *Medical Engineering and Physics*, vol. 32, no. 2, p. 155–160, 2010.

[18] J. M. P. Quiroga, W. Wilson, K. Ito, and C. C. van Donkelaar, "Relative contribution of articular cartilage's constitutive components to load support depending on strain rate," *Biomechanics and Modeling in Mechanobiology*, vol. 16, p. 151–158, Jul 2017.

[19] N. Sakai, C. Hashimoto, S. Yarimitsu, Y. Sawae, M. Komori, and T. Murakami, "A functional effect of the superficial mechanical properties of articular cartilage as a load bearing system in a sliding condition," *Biosurface and Biotribology*, vol. 2, p. 26–39, Mar 2016.

[20] W. M. Lai and V. C. Mow, "Drag-induced compression of articular cartilage during a permeation experiment," *Biorheology*, vol. 17, no. 1–2, p. 111–123, 1980.

[21] M. Freutel, H. Schmidt, L. Dürselen, A. Ignatius, and F. Galbusera, "Finite element modeling of soft tissues: Material models, tissue interaction and challenges," *Clinical Biomechanics*, vol. 29, no. 4, p. 363–372, 2014.

[22] J. Y. Bae, K. S. Park, J. K. Seon, D. S. Kwak, I. Jeon, and E. K. Song, "Biomechanical analysis of the effects of medial meniscectomy on degenerative osteoarthritis," *Medical and Biological Engineering and Computing*, vol. 50, no. 1, p. 53–60, 2012.

[23] B. Jones, C. T. Hung, and G. Ateshian, "Biphasic analysis of cartilage stresses in the patellofemoral joint," *Journal of Knee Surgery*, vol. 29, no. 2, p. 92–98, 2015.

[24] V. C. Mow and X. E. Guo, "Mechano-electrochemical properties of articular cartilage: Their inhomogeneities and anisotropies," *Annual Review of Biomedical Engineering*, vol. 4, p. 175–209, Aug 2002.

[25] M. E. Stender, C. B. Raub, K. A. Yamauchi, R. Shirazi, P. Vena, R. L. Sah, S. J. Hazelwood, and S. M. Klisch, "Integrating qplm and biomechanical test data with an anisotropic fiber distribution model and predictions of tgf-$\beta$1 and igf-1 regulation of articular cartilage fiber modulus," *Biomechanics and Modeling in Mechanobiology*, vol. 12, p. 1073–1088, Nov 2012.

[26] J. M. Párraga Quiroga, W. Wilson, K. Ito, and C. C. van Donkelaar, "The effect of loading rate on the development of early damage in articular cartilage," *Biomechanics and Modeling in Mechanobiology*, vol. 16, no. 1, p. 263–273, 2017.

[27] V. C. Mow, S. C. Kuei, W. M. Lai, and C. G. Armstrong, "Biphasic creep and stress relaxation of articular cartilage in compression: Theory and experiments," *Journal of Biomechanical Engineering*, vol. 102, p. 73, Feb 1980.

[28] W. Wilson, J. M. Huyghe, and C. C. Van Donkelaar, "Depth-dependent compressive equilibrium properties of articular cartilage explained by its composition," *Biomechanics and Modeling in Mechanobiology*, vol. 6, p. 43–53, Jan 2007.

[29] L. P. Li and W. Herzog, "The role of viscoelasticity of collagen fibers in articular cartilage: Theory and numerical formulation," *Biorheology*, vol. 41, no. 3–4, p. 181–194, 2004.

[30] A. Benninghoff, "Form und bau der gelenkknorpel in ihren beziehungen zur funktion," *Zeitschrift für Anatomie und Entwicklungsgeschichte*, vol. 76, no. 1–3, p. 43–63, 1925.

[31] W. Wilson, C. C. van Donkelaar, B. van Rietbergen, K. Ito, and R. Huiskes, "Stresses in the local collagen network of articular cartilage: a poroviscoelastic fibril-reinforced finite element study.," *Journal of biomechanics*, vol. 37, p. 357–66, Mar 2004.

[32] W. Wilson, C. van Donkelaar, B. van Rietbergen, and R. Huiskes, "A fibril-reinforced poroviscoelastic swelling model for articular cartilage," *Journal of Biomechanics*, vol. 38, p. 1195–1204, Jun 2005.

[33] S. R. Oungoulian, S. S. Chen, A. Davol, R. L. Sah, and S. M. Klisch, *Extended two compartmental swelling stress model and isotropic cauchy stress equation for articular cartilage proteoglycans*, p. 847–848. 2007.

[34] M. D. Buschmann and A. J. Grodzinsky, "A molecular model of proteoglycan-associated electrostatic forces in cartilage mechanics," *Journal of Biomechanical Engineering*, vol. 117, p. 179, May 1995.

[35] G. A. Ateshian, W. H. Warden, J. J. Kim, R. P. Grelsamer, and V. C. Mow, "Finite deformation biphasic material properties of bovine articular cartilage from confined compression experiments," *Journal of Biomechanics*, vol. 30, no. 11, p. 1157–1164, 1997.

[36] M. H. Holmes and V. C. Mow, "The nonlinear characteristics of soft gels and hydrated connective tissues in ultrafiltration," *Journal of Biomechanics*, vol. 23, no. 11, p. 1145–1156, 1990.

[37] A. van der Voet, "A comparison of finite element codes for the solution of biphasic poroelastic problems.," *Proceedings of the Institution of Mechanical Engineers. Part H, Journal of engineering in medicine*, vol. 211, no. 2, p. 209–11, 1997.

[38] J. Z. Wu and W. Herzog, "Finite element simulation of location- and time-dependent mechanical behavior of chondrocytes in unconfined compression tests.," *Annals of biomedical engineering*, vol. 28, no. 3, p. 318–30, 2000.

[39] L. Borchers and P. Reichart, "Three-dimensional stress distribution around a dental implant at different stages of interface development," *Journal of Dental Research*, vol. 62, p. 155–159, Feb 1983.

[40] R. Brocklehurst, M. T. Bayliss, A. Maroudas, H. L. Coysh, M. A. Freeman, P. A. Revell, and S. Y. Ali, "The composition of normal and osteoarthritic articular cartilage from human knee joints. with special reference to unicompartmental replacement and osteotomy of the knee," *Journal of Bone and Joint Surgery - Series A*, vol. 66, no. 1, p. 95–106, 1984.

[41] S. S. Chen, Y. H. Falcovitz, R. Schneiderman, A. Maroudas, and R. L. Sah, "Depth-dependent compressive properties of normal aged human femoral head articular cartilage: relationship to fixed charge density," *Osteoarthritis and Cartilage*, vol. 9, p. 561–569, Aug 2001.

[42] P. L. Mente and J. L. Lewis, "Elastic modulus of calcified cartilage is an order of magnitude less than that of subchondral bone," *Journal of Orthopaedic Research*, vol. 12, p. 637–647, Sep 1994.

[43] E. F. Morgan and T. M. Keaveny, "Dependence of yield strain of human trabecular bone on anatomic site," *Journal of Biomechanics*, vol. 34, p. 569–577, May 2001.

[44] E. A. Nauman, K. E. Fong, and T. M. Keaveny, "Dependence of intertrabecular permeability on flow direction and anatomic site," *Annals of Biomedical Engineering*, vol. 27, p. 517–524, Jul 1999.

[45] L. A. Setton, V. C. Mow, and D. S. Howell, "Mechanical behavior of articular cartilage in shear is altered by transection of the anterior cruciate ligament," *Journal of Orthopaedic Research*, vol. 13, p. 473–482, Jul 1995.

[46] X. Wei, T. Räsänen, and K. Messner, "Maturation-related compressive properties of rabbit knee articular cartilage and volume fraction of subchondral tissue," *Osteoarthritis and Cartilage*, vol. 6, p. 400–409, Nov 1998.

[47] M. Taffetani, M. Griebel, D. Gastaldi, S. M. Klisch, and P. Vena, "Poroviscoelastic finite element model including continuous fiber distribution for the simulation of nanoindentation tests on articular cartilage," *Journal of the Mechanical Behavior of Biomedical Materials*, vol. 32, p. 17–30, 2014.

[48] H. Lipshitz, R. Etheredge, and M. Glimcher, "In vitro wear of articular cartilage," *The Journal of Bone & Joint Surgery*, vol. 57, no. 4, p. 527–534, 1975.

[49] J. Rieppo, "Spatial determination of water, collagen and proteogycan content by fourier transform infrared imaging and digital densitometry," *50th Annual meeting of the Orthopaedic Research Society*, no. Evo 5173, p. Poster No: 1021, 2004.

[50] E. M. Shapiro, A. Borthakur, J. H. Kaufman, J. S. Leigh, and R. Reddy, "Water distribution patterns inside bovine articular cartilage as visualized by 1h magnetic resonance imaging," *Osteoarthritis and Cartilage*, vol. 9, p. 533–538, Aug 2001.

[51] P. Julkunen, W. Wilson, J. S. Jurvelin, J. Rieppo, C. J. Qu, M. J. Lammi, and R. K. Korhonen, "Stress-relaxation of human patellar articular cartilage in unconfined compression: Prediction of mechanical response by tissue composition and structure," *Journal of Biomechanics*, vol. 41, no. 9, p. 1978–1986, 2008.

[52] R. K. Korhonen, M. S. Laasanen, J. Töyräs, R. Lappalainen, H. J. Helminen, and J. S. Jurvelin, "Fibril reinforced poroelastic model predicts specifically mechanical behavior of normal, proteoglycan depleted and collagen degraded articular cartilage," *Journal of Biomechanics*, vol. 36, p. 1373–1379, Sep 2003.

[53] M. E. Mononen, P. Julkunen, J. Töyräs, J. S. Jurvelin, I. Kiviranta, and R. K. Korhonen, "Alterations in structure and properties of collagen network of osteoarthritic and repaired cartilage modify knee joint stresses," *Biomechanics and Modeling in Mechanobiology*, vol. 10, no. 3, p. 357–369, 2011.

[54] N. Nguyen and A. M. Waas, "Nonlinear, finite deformation, finite element analysis," *Zeitschrift fur Angewandte Mathematik und Physik*, vol. 67, no. 3, p. 35, 2016.

[55] S. S. Pawaskar, J. Fisher, and Z. Jin, "Robust and general method for determining surface fluid flow boundary conditions in articular cartilage contact mechanics modeling," *Journal of Biomechanical Engineering*, vol. 132, no. 3, p. 031001, 2010.

[56] R. K. Korhonen, M. S. Laasanen, J. Töyräs, J. Rieppo, J. Hirvonen, H. J. Helminen, and J. S. Jurvelin, "Comparison of the equilibrium response of articular cartilage in unconfined compression, confined compression and indentation," *Journal of Biomechanics*, vol. 35, p. 903–909, Jul 2002.

[57] R. M. Schinagl, D. Gurskis, A. C. Chen, and R. L. Sah, "Depth-dependent confined compression modulus of full-thickness bovine articular cartilage," *Journal of Orthopaedic Research*, vol. 15, no. 4, p. 499–506, 1997.

[58] D. L. Robinson, M. E. Kersh, N. C. Walsh, D. C. Ackland, R. N. de Steiger, and M. G. Pandy, "Mechanical properties of normal and osteoarthritic human articular cartilage," *Journal of the Mechanical Behavior of Biomedical Materials*, vol. 61, p. 96–109, 2016.

[59] J. Pan, X. Zhou, W. Li, J. E. Novotny, S. B. Doty, and L. Wang, "In situ measurement of transport between subchondral bone and articular cartilage," *Journal of Orthopaedic Research*, vol. 27, p. 1347–1352, Oct 2009.

[60] A. Connolly, D. FitzPatrick, J. Moulton, J. Lee, and A. Lerner, "Tibiofemoral cartilage thickness distribution and its correlation with anthropometric variables," *Proceedings of the Institution of Mechanical Engineers, Part H: Journal of Engineering in Medicine*, vol. 222, p. 29–39, Jan 2008.

[61] C. J. Bell, E. Ingham, and J. Fisher, "Influence of hyaluronic acid on the time-dependent friction response of articular cartilage under different conditions," *Proceedings of the Institution of Mechanical Engineers, Part H: Journal of Engineering in Medicine*, vol. 220, p. 23–31, Jan 2006.

[62] H. Mohammadi, K. Mequanint, and W. Herzog, *A p-type finite element solution for the simulation of O 2 transport in articular cartilage tissue: Heterogeneous and porous media*, vol. 225, p. 1003–1014. SAGE PublicationsSage UK: London, England, Oct 2011.

[63] D. M. Pierce, M. J. Unterberger, W. Trobin, T. Ricken, and G. A. Holzapfel, "A microstructurally based continuum model of cartilage viscoelasticity and permeability incorporating measured statistical fiber orientations," *Biomechanics and Modeling in Mechanobiology*, vol. 15, p. 229–244, Feb 2016.

[64] H. Sadeghi, D. M. Espino, and D. E. Shepherd, "Variation in viscoelastic properties of bovine articular cartilage below, up to and above healthy gait-relevant loading frequencies," *Proceedings of the Institution of Mechanical Engineers, Part H: Journal of Engineering in Medicine*, vol. 229, p. 115–123, Feb 2015.

[65] L. Wang, D. N. Kalu, J. Banu, J. B. Thomas, N. Gabriel, and K. Athanasiou, "Effects of ageing on the biomechanical properties of rat articular cartilage," *Proceedings of the Institution of Mechanical Engineers, Part H: Journal of Engineering in Medicine*, vol. 220, p. 573–578, Apr 2006.

[66] J. Bonet and R. D. Wood, *Nonlinear continuum mechanics for finite element analysis*, vol. 9780521838. Cambridge University Press, 2nd ed., 2008.

## Appendix

In this appendix, the details of the consistent Jacobian tensor derivation for the fibrillar and non-fibrillar AC matrix constituents are presented via a similar approach of the GAG constituent derivation [25,47]. Recalling (11) and using (2), the 2nd Piola–Kirchhoff stress tensor of the fibrillar constituent was simply derived as

$$S_{ij}^{COL} = \phi_0^S \sum_{I=1}^{9} \rho_C^I \left( \frac{E_0 + E_\varepsilon \varepsilon_F^I}{\lambda^I} \varepsilon_F^I N_i^I N_j^I \right) \tag{16}$$

Where $N_i^I$ is the initial fibril direction in the *Ith* fibril that is related to the right Cauchy-Green deformation tensor by

$$N_i^I C_{ij} N_j^I = \left(\lambda^I\right)^2 \tag{17}$$

Recalling (10) and using (16), the fibrillar material elasticity tensor was derived as

$${}^4\widetilde{C}_{ijkr}^{COL} = \phi_0^S \sum_{I=1}^{9} \left( \frac{\rho_C^I}{\lambda^I} \left[ \left(E_0 + 2E_\varepsilon \varepsilon_F^I\right) \left( \frac{\partial \varepsilon_F^I}{\partial C_{kr}} + \frac{\partial \varepsilon_F^I}{\partial C_{rk}} \right) - \frac{E_0 + E_\varepsilon \varepsilon_F^I}{\lambda^I} \left( \frac{\partial \lambda^I}{\partial C_{kr}} + \frac{\partial \lambda^I}{\partial C_{rk}} \right) \varepsilon_F^I \right] N_i^I N_j^I \right) \tag{18}$$

Also, differentiation of the fibrillar logarithmic strain with respect to the right Cauchy-Green deformation tensor yields

$$\frac{\partial \varepsilon_F^I}{\partial \mathbf{C}} = \frac{1}{\lambda^I} \frac{\partial \lambda^I}{\partial \mathbf{C}} \tag{19}$$

And differentiation of equation (17) with respect to elongation yields

$$\frac{\partial \lambda^I}{\partial C_{ij}} = \frac{1}{2\lambda^I} N_i^I N_j^I \tag{20}$$

Substituting (19) and (20) into (18) and recalling (9), the fibrillar matrix spatial elasticity tensor yields (14). On the other hand, the non-fibrillar matrix material elasticity tensor was derived by a similar approach as

$$\begin{aligned} {}^4\widetilde{\mathbf{C}}_{MAT} = -2G_M \left(1 - \rho_C^{TOT}\right) \phi_0^S \Bigg( & \mathbf{C}^{-1} \frac{\partial \left( J^{2/3} + \frac{lnJ}{6} \left[ \frac{3\phi_0^S}{J - \phi_0^S} \left( \frac{JlnJ}{J - \phi_0^S} - 2 \right) - 4 \right] \right)}{\partial \mathbf{C}} \\ & + \left( J^{2/3} + \frac{lnJ}{6} \left[ \frac{3\phi_0^S}{J - \phi_0^S} \left( \frac{JlnJ}{J - \phi_0^S} - 2 \right) - 4 \right] \right) \frac{\partial \mathbf{C}^{-1}}{\partial \mathbf{C}} \Bigg) \end{aligned} \tag{21}$$

This equation requires the following differentiations [66]

$$\frac{\partial C_{ij}^{-1}}{\partial C_{kr}} = -\frac{1}{2} \left( C_{ik}^{-1} C_{jr}^{-1} + C_{ir}^{-1} C_{jk}^{-1} \right) \tag{22}$$

$$\frac{\partial (J)}{\partial \mathbf{C}} = \frac{J}{2} \mathbf{C}^{-T} \tag{23}$$

Substituting (22) and (23) into (21) and recalling (9), the non-fibrillar matrix spatial elasticity tensor yields (15).